



This manuscript has been authored by UT-Battelle, LLC under Contract No. DE-AC05-00OR22725 with the U.S. Department of Energy. The United States Government retains and the publisher, by accepting the article for publication, acknowledges that the United States Government retains a non-exclusive, paid-up, irrevocable, world-wide license to publish or reproduce the published form of this manuscript, or allow others to do so, for United States Government purposes. The Department of Energy will provide public access to these results of federally sponsored research in accordance with the DOE Public Access Plan (http://energy.gov/downloads/doe-public-access-plan).

Crystals 2022, 12, x. https://doi.org/10.3390/xxxxx

Article

Lattice parameter evolution during the β -to- α and β -to- ω transformations of iron and aluminum modified Ti-11Cr(at.%)

JoAnn Ballor ¹, Jonathan D. Poplawsky ², Arun Devaraj ³, Scott Misture ⁴, and Carl J. Boehlert ^{1,*}

- Department of Chemical Engineering and Material Science, Michigan State University, East Lansing, Michigan, United States; boehlert@msu.edu
- ² Center for Nanophase Materials Sciences, Oak Ridge National Laboratory, Oak Ridge, Tennessee, United States; poplawskyj@ornl.gov
- ³ Physical and Computational Sciences Directorate, Pacific Northwest National Laboratory, Richland, Washington, 99352, United States; arun.devaraj@pnnl.gov
- Inamori School of Engineering, Alfred University, Alfred, New York, United States; misture@alfred.edu
- * Correspondence: boehlert@msu.edu

Abstract: β-titanium (β-Ti) alloys are useful in diverse industries because their mechanical properties can be tuned by transforming the metastable β -phase into other metastable and stable phases. Relationships between lattice parameter and β-Ti alloy concentrations have been explored, but the lattice parameter evolution during β-phase transformations is not well understood. In this work, the β-Ti alloys, Ti-11Cr, Ti-11Cr-0.85Fe, Ti-11Cr-5.3Al, and Ti-11Cr-0.85Fe-5.3Al (all in at.%) underwent a 400°C aging treatment for up to 12 hours to induce the β-to- ω and β-to- α phase transformations. Phase identification and lattice parameters were measured in-situ using high-temperature X-ray diffraction. Phase compositions were measured ex-situ using atom probe tomography. During the phase transformations, Cr and Fe diffused from the ω and α phases into the β matrix, and the β -phase lattice parameter exhibited a corresponding decrease. The decrease in β -phase lattice parameter affected the α - and ω -phase lattice parameters. The α phase in the Fe-free alloys exhibited α -phase c/a ratios close to those of pure Ti. A larger β -phase composition change in Ti-11Cr resulted in larger ω -phase lattice parameter changes than in Ti-11Cr-0.85Fe. This work illuminates the complex relationship between diffusion, composition, and structure for these diffusive/displacive transformations

Keywords: lattice parameters; phase transformations; titanium alloys; X-ray analysis; atom probe tomography; characterization

Citation: Lastname, F.; Lastname, F.; Lastname, F. Title. *Crystals* **2022**, *12*, x. https://doi.org/10.3390/xxxxx

Academic Editor: Firstname Last-

Received: date Accepted: date Published: date

Publisher's Note: MDPI stays neutral with regard to jurisdictional claims in published maps and institutional affiliations.



Copyright: © 2022 by the authors. Submitted for possible open access publication under the terms and conditions of the Creative Commons Attribution (CC BY) license (https://creativecommons.org/licenses/by/4.0/).

1. Introduction

 β -Ti alloys are used in diverse industries because they can exhibit a wide range of mechanical properties through transforming the metastable body-centered-cubic β phase into other metastable and stable phases, such as the metastable ω phase and the stable α phase. Due to these transformations, β -Ti alloys can exhibit high strengths that are attractive for structural applications [1]. Because of their high strength-to-weight ratios, β -Ti alloys are also a promising option for lightweighting in the automotive industry [2]. However, the relatively high cost of Ti alloys compared to steels or aluminum (Al) alloys impedes their widespread use. One way to reduce the cost of β -Ti alloys is by including less expensive alloying elements, such as chromium (Cr), iron (Fe), and Al. To choose the best combination of alloying elements for achieving desired mechanical properties, a thorough understanding of how alloy composition and processing can affect the microstructure and mechanical properties is necessary.

To retain the metastable β phase upon quenching, β -phase stabilizing elements are needed. To compare the compositions of β -Ti alloys, the molybdenum equivalency (Mo-Eq.) equation was developed, which provides an amount of Mo that could replace the

elements in the alloy and provide the same β -phase stability [3]. The average atomic radii and average electron d-shell energy (Md) of the alloy compositions are also important to alloy design, as they are related to the deformation mechanisms in β -Ti alloys. Average atomic radius, average Md, and composition (through Mo-Eq.) show a clear interrelationship, see Figure 1.

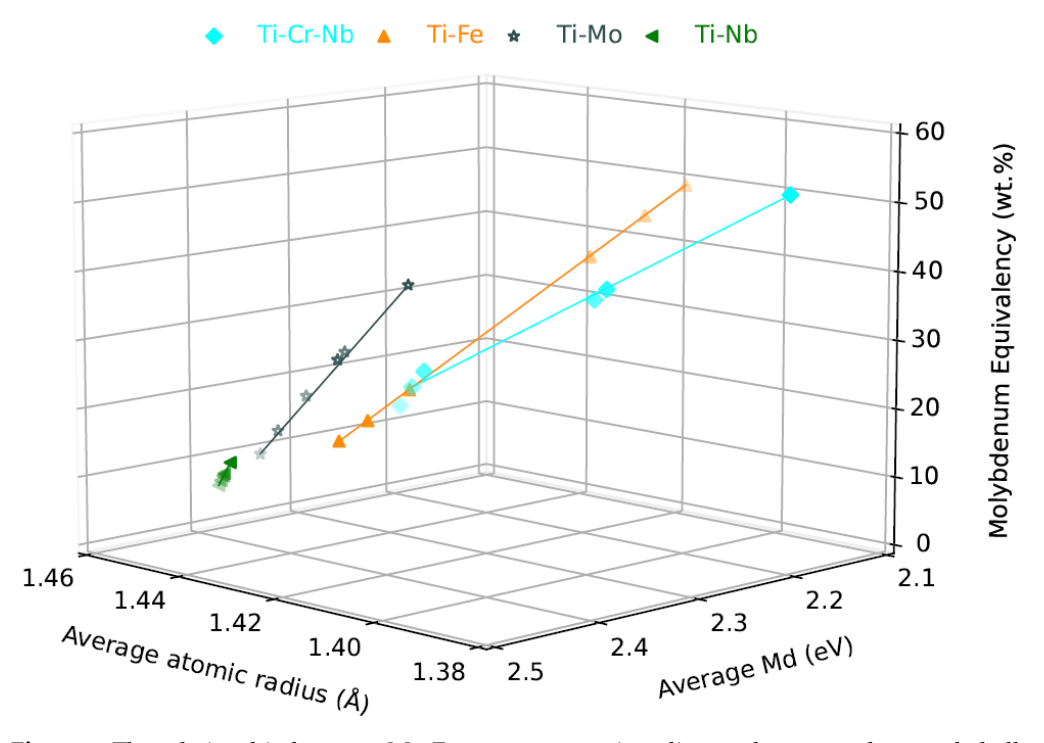


Figure 1. The relationship between Mo-Eq, average atomic radius, and average electron d-shell energy (Md) for the β -Ti alloys Ti-Cr-Nb [4], Ti-Fe [5], Ti-Mo [6], and Ti-Nb [7].

In addition to the relationships shown in Figure 1, the β -phase lattice parameter (a β) is related to Mo-Eq. (as well as the average radius and Md) as a β decreases with increasing Mo, Cr, and Fe content [4–6], increases with increasing Nb contents between 5 and 22at.% [7], and remains relatively constant for Nb contents between 22-35at.% [8].

These lattice parameter changes have been documented in fully β -phase microstructures, but have not been fully explored in multiphase microstructures. β -phase alloys can be strengthened through aging due to the precipitation of the ω and α phases through a diffusive/displacive phase transformation mechanism, where the β -phase stabilizers diffuse from the ω - and α -phase precipitates into the surrounding β matrix [9,10]. This diffusion changes the β -phase Mo-Eq. during the phase transformations, and thus affects the average Md, average atomic radius, and lattice parameter of the β phase. Similarly, the α -phase lattice parameters have also been reported to change during the displacive/diffusive phase transformation during aging [11], and changes in α - and β -phase lattice parameters with changing phase compositions have been reported in α + β alloys Ti-6Al-4V(wt.%) [12] and Ti-6Al-6V-2Sn(wt.%) [13], but are not well-reported in metastable β alloys.

Diffusion is important to both β -to- α and β -to- ω transformations because they are both displacive/diffusive transformations. The metastable ω -phase composition is particularly important as its precipitation can be affected by the addition of elements such as tin and oxygen, as athermal ω -phase prefers Ti-rich compositions, and diffusion during the isothermal ω -phase transformation makes the β -to- ω transformation irreversible [14–17]. Understanding the evolution of the lattice parameters of each phase during the phase transformations is critical for understanding the phase misfit, which can affect the growth and morphology of the transforming phases [18], the local deformation mechanisms

[19,20], and the residual stress in materials [21,22]. The ledges of the ω phase at the ω/β boundary are favorable locations for the ω -assisted α -phase transformation [23–27]. The ω -assisted α -phase transformation is desired due to the nanoscale α -phase that forms and the corresponding superior mechanical properties [28–31]. The misfit and ω/α interfaces have been investigated using high-resolution imaging techniques, but lattice parameters of the phases are not always reported, and are usually ex-situ (after the aging has occurred). High-temperature XRD offers a unique opportunity to monitor the lattice parameter transformations in the bulk material during aging. The small size of the ω and α precipitates do pose a challenge to the technique, but the knowledge gained through the insitu experiment is worth the investigation. Similarly, these small precipitates pose a challenge to composition measurement, so atom probe tomography, with its nanoscale resolution, was chosen to investigate the details of the precipitates' compositions. As the phase diagrams for the tertiary and quaternary alloys are not yet established, this work also adds to the knowledge of phases and the associated phase fields in these more complex systems.

In this work, the evolution of the β -, α -, and ω -phase lattice parameters during the β -to- ω and β -to- α phase transformations are explored in the Ti-Cr alloy system, which undergoes the β -to- ω and β -to- α phase transformations [32–34]. A base alloy of Ti-11Cr(at.%) alloy was chosen for this study, and the β -phase stabilizer, Fe, and the α -phase stabilizer, Al, were added to determine their effects on the phase transformations and the lattice parameters with aging time. In-situ high-temperature X-ray diffraction (HTXRD) was performed to investigate both the phase transformations and the lattice parameters of all the phases present during 400°C aging, and atom probe tomography (APT) was used to determine the nanoscale composition of each phase in each alloy. Through the combination of APT and HTXRD, the relationship between the lattice parameter and phase composition during the β -to- ω and β -to- α phase transformations is determined for Fe- and Almodified Ti-11Cr(at.%)

2. Materials and Methods

Ti-11Cr(at.%) (TC), Ti-11Cr-0.85Fe(at.%) (TCF), Ti-11Cr-5.3Al(at.%) (TCA), and Ti-11Cr-0.85Fe-5.3Al(at.%) (TCFA) were levitation melted in a 2kg, 90Dx80L LEV levitation induction furnace and hot forged at approximately 1047° C into $25 \times 60 \times 250$ -mm³ blocks, then homogenized using a 900°C anneal for 1 h in vacuum, followed by ice-water quenching at an estimated cooling rate of 34.7° C/s. All of these processing steps were performed at Daido Steel Company, Ltd. (Nagoya, Japan). The measured composition of each alloy was reported earlier [35]. All alloy concentrations in this work are reported in atomic percent. A 400°C aging heat treatment was chosen to induce the ω - and α -phase transformations, as Ti-Cr alloys have formed both phases after aging at that temperature [32–34].

For APT sample preparation, samples were cut from the forged alloy blocks using a diamond saw. These sample were then aged at 400°C in a vacuum followed by air quenching. TC and TCFA were aged for 0.75, 1.5, 3, 6, and 12 h, while TCF and TCA were aged for 0.75, 1.5, and 12 h. After aging, the samples were metallographically polished to a mirror finish according to [36]. APT needle specimens were extracted using the FIB-based lift-out and annular milling method described in [37]. A CAMECA local electrode atom probe (LEAP) 4000X HR system was used for all APT data collection. Pulsed-voltage mode with a 200kHz pulse frequency, 50 K specimen temperature, pulse fraction of 0.2, and a detection rate of 0.5% was used for all the 12 h aged samples, and the 0.75 h and 1.5 h aged TC and TCFA samples. Pulsed-laser mode with a 50 pJ laser energy, 200 kHz pulse frequency, 30 K specimen temperature, and a detection rate of 0.5% was used for all the other samples.

Samples for HTXRD were cut using an electrodischarge machine and polished using 320 grit silicon carbide paper to remove any macroscopic surface defects or oxides. The final sample dimensions were approximately 17mm x 17mm x 1.1mm. HTXRD was performed using a Bruker-AXS (Madison, WI) D8 diffractometer with an automatic sample

changer, a Vantec linear position-sensitive detector, $\text{Cu-K}\alpha$ radiation, and an Anton-Paar HTK1200 furnace with ultra-high-purity nitrogen gas to prevent sample oxidation during heating. XRD peaks associated with Ti nitrides were not observed, so it is believed that nitriding did not occur. The room temperature (RT) XRD scan of the β -homogenized condition exhibited only the (101) β , (200) β , and (211) β peaks, confirming the fully β -phase microstructure. The heating rate to 400°C was 30°C/min. Data was collected in-situ over a 2 θ range of 25° to 75° every 0.5 h during the 12 h aging period with a scan rate of 2°/min.

For each alloy, Rietveld analysis was performed on the HTXRD data to determine the lattice parameters of the β , α , and ω phases after each 0.5 h time step. The Rietveld refinement and lattice parameter calculations were accomplished for TCF, TCA, and TCFA using the Topas software package (Bruker-AXS). The Rietveld lattice parameter refinement for TC was accomplished using software suite PDXL version 2 [38], and the weighted-profile residual (Rwp) for each Rietveld analysis was between 4.87% and 7.85%. For TC, only the lattice parameters were refined. For TCF, TCA, and TCFA, both the lattice parameters and the profiles were refined. Table 1 contains the crystallographic information of the phases considered for the Rietveld refinement.

Table 1. The crystallographic data of the β , α , and ω phases used for the Rietveld refinement.

| Phase | e a (Å) | b (Å) |) c (Å) | Structure | Space Group | Atomic Positions (x,y,z) | Reference |
|----------|---------|-------|---------|------------------------|--------------|-----------------------------------------|-----------|
| β | 3.21 | - | - | Cubic | Im3m(229) | (0,0,0) $(1/2,1/2,1/2)$ | [39] |
| α | 2.9508 | - | 4.6855 | Hexagonal close-packed | P63/mmc(194) | (0,0,0) $(1/3,2/3,1/2)$ | [40] |
| ω | 4.6 | - | 2.82 | Hexagonal | P6/mmm(191) | (0,0,0) $(1/3,2/3,1/2)$ $(2/3,1/3,1/2)$ | [41] |

3. Results

3.1. Microstructural evolution evaluated by in-situ high-temperature XRD

The in-situ HTXRD data revealed that phase transformations occurred during the first 0.5 h at 400°C. β -, ω -, and α -phase peaks were observed in the 0.5 h XRD profiles of TC and TCF, see Figure 2(a,b) respectively. Only β - and α -phase peaks were observed in the 0.5 h XRD profiles of TCA and TCFA, see Figure 2(c,d), respectively. The lack of ω -phase peaks in TCA and TCFA suggest that the Al addition promoted the formation of the α phase preferentially over the ω phase.

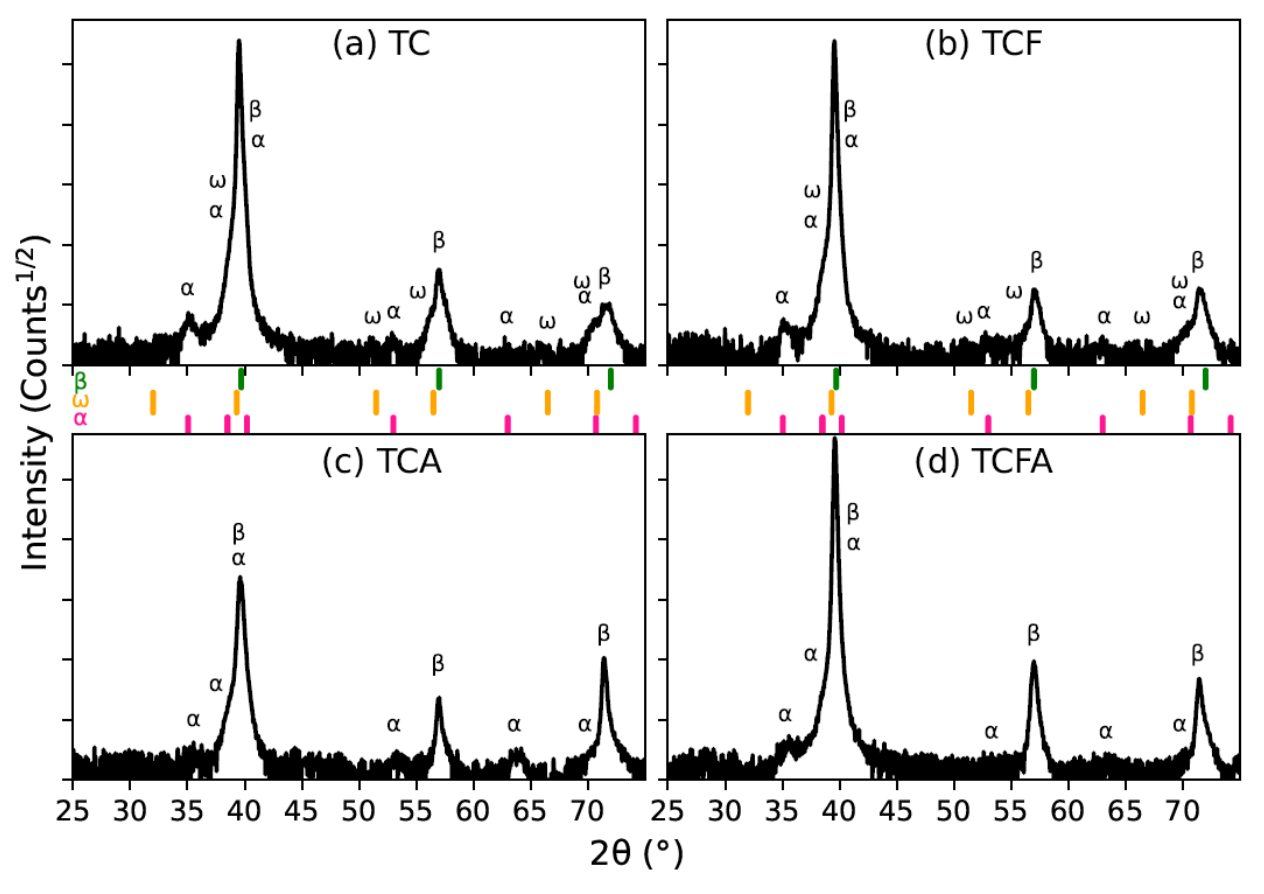


Figure 2. HTXRD intensity versus 2θ plots after 0.5 h at 400°C showing the β -, α -, and ω -phase peaks for (a) TC and (b) TCF, and the β - and α -phase peaks for (c) TCA and (d) TCFA.

The HTXRD data, taken every 0.5 h during the 400°C aging, revealed the evolution of the phase peaks in each alloy with aging time. Heatmap-style waterfall plots were used to reveal the peak evolutions as a function of both 20 diffraction angle (°) and aging time (h). In the two-phase TCA and TCFA the β -phase peaks appeared to shift to high 20 values with increased aging time, while the α -phase peaks appeared to remain at approximately the same angles, see Figure 3. The peak shift was more pronounced at higher 20 values and lower aging times. No ω -phase peaks were observed in any of the TCA or TCFA profiles.

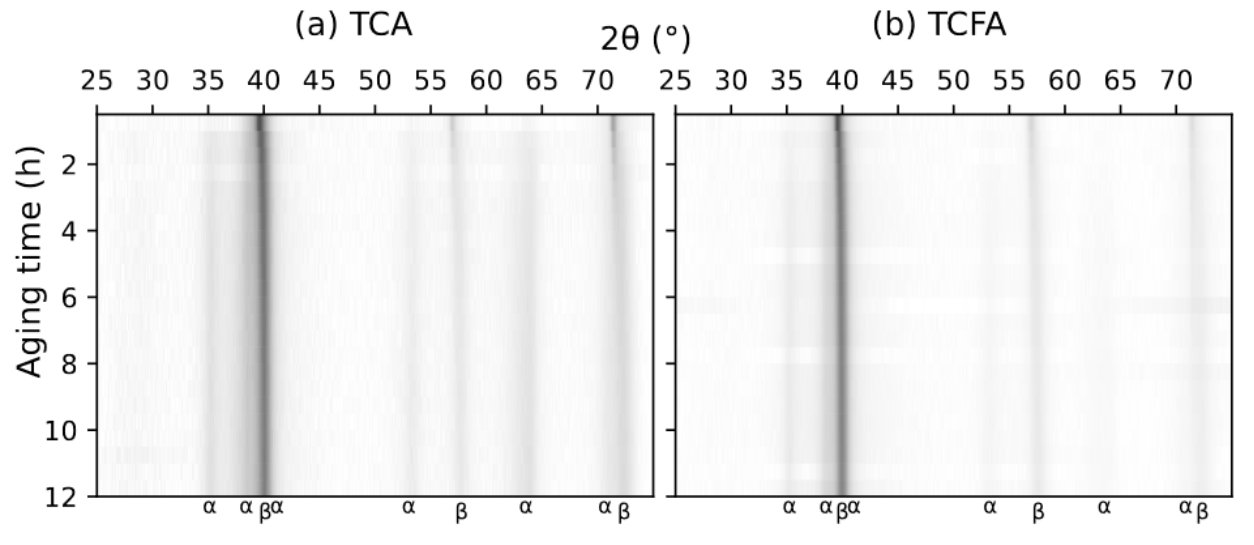


Figure 3. The experimental profiles for (a) TCA and (b) TCFA presented as a function of aging time, where darker values indicate higher intensities. Each peak is labeled with its corresponding phase along the bottom of the axis.

The peak overlap in the TC and TCF data made it difficult to determine the evolution of each peak with aging time. Rietveld analysis was performed to deconvolute the contributions from the β , ω , and α phases for each XRD profile. Figure 4 shows the deconvolution of the TC XRD profile after 3 h aging at 400°C. This deconvolution is representative of the deconvolution for each of the alloys.

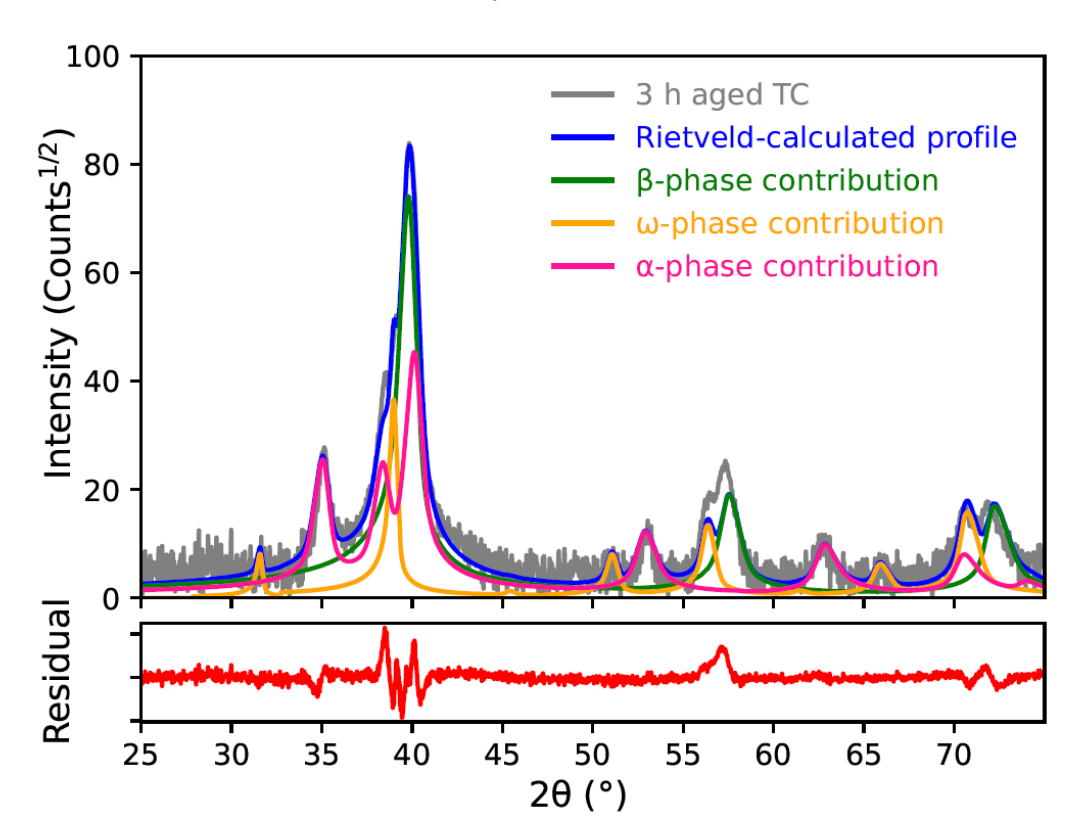


Figure 4. The experimental XRD profile of TC at 1.5 h at 400°C, with the Rietveld-calculated profile (blue) with the individual contributions from the β (green), ω (orange), and α (pink) phases. The calculated profile is the sum of the individual contributions from each phase, and the residual shows the difference between the experimental and the calculated profiles.

Through the deconvolution of the peaks, it was possible to determine the evolution of each phase's peak in the TC and TCF data, see Figure 5(a,b) respectively. Plotting the deconvoluted profiles show that the β -phase peaks of TC and TCF also appear to shift to higher angles with increased aging times. The α -phase peaks appear to remain at approximately the same angles like TCA and TCFA. The ω -phase peaks also appear to remain at approximately the same angles throughout the 12 h heat treatment in TC. The ω -phase peaks are not clearly visible after 7.5 h at 400°C in TCF, suggesting that the Fe addition in TCF limits the stability of the metastable ω phase compared to TC. Although it is possible ω -phase remained in TCF past 7.5 h, during the deconvolution of the TCF 8-12 h profiles the Rietveld analysis used the ω -phase profile as a smoothing function to decrease the residual between the calculated and experimental profiles, which led to unrealistic peak locations for all three phases. Thus, the ω -phase was removed from the iterative Rietveld analysis of the TCF profiles for times from 8-12 h.

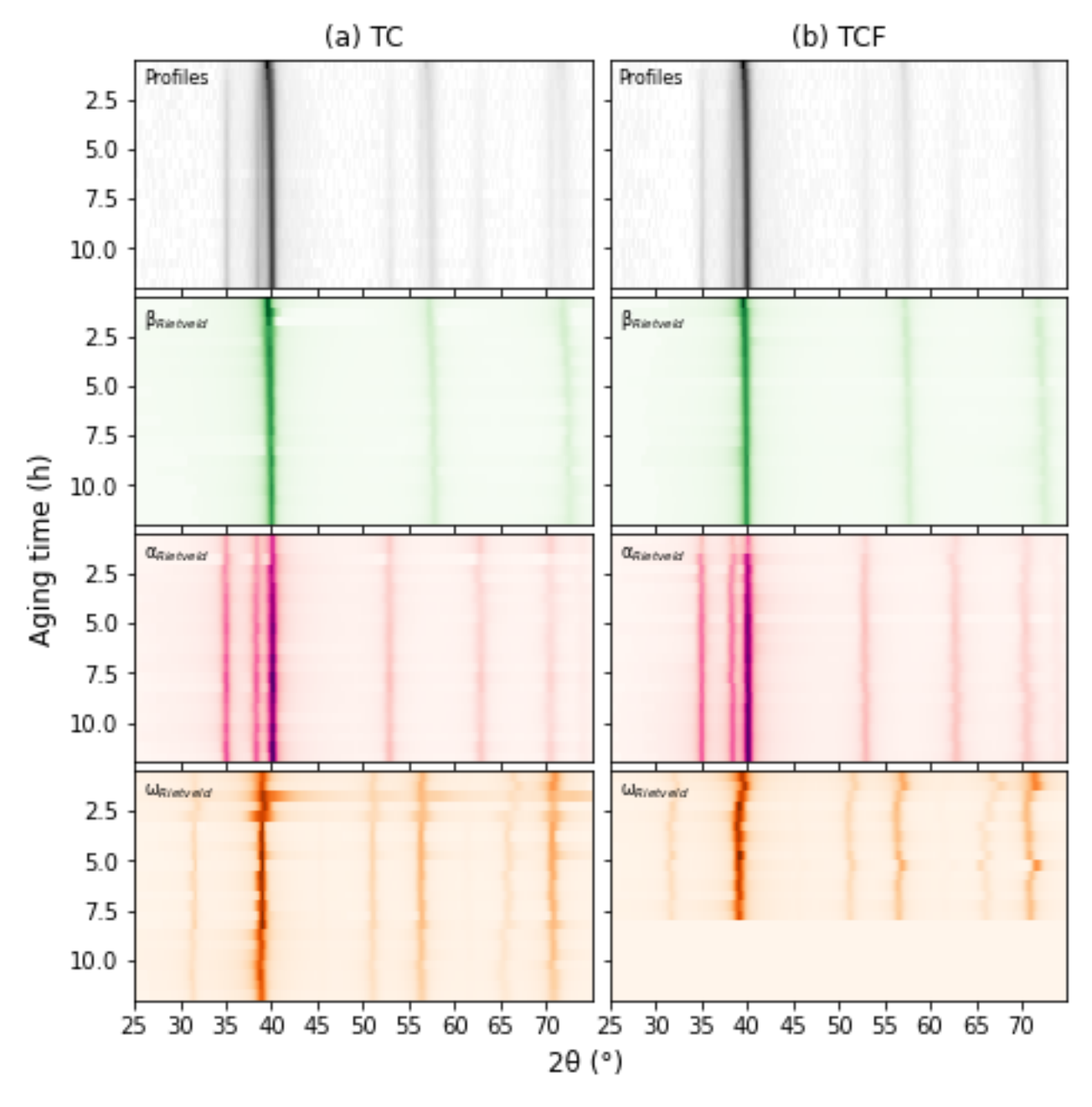


Figure 5. The experimental profiles (top) and the Rietveld deconvolutions of the β (green), α (pink), and ω (orange) phases during the 400°C HTXRD experiment for (a) TC and (b) TCF, where darker values indicate higher intensities. The ω -phase peaks, which were not visible for TCF after 7.5 h at 400°C, were removed from the Rietveld analysis after 7.5 h. This Rietveld deconvolution has previously been presented in Ballor et al. [42].

The evolution of the phase peaks in each alloy suggests that a_{β} decreased with increasing aging time, while the α - and ω -phase lattice parameters remained approximately constant. Lattice parameters were determined as part of the Rietveld analysis, and peak overlap and peak broadness made certain profiles difficult to refine. The TCA profiles were particularly difficult to refine during the later aging times due to peak broadness. In TC and TCF the Rietveld analysis tended to reverse the ω - and α -phase peak locations due to the overlap between the β , ω , and α peaks. This reversal led to calculated lattice parameters and phase profiles that were unrealistic according to the literature. When these inaccuracies occurred, the Rietveld analysis was performed again, holding the parameters corresponding to peak shape and location constant, when necessary, to prevent

the reversals. This generally followed the pattern of holding the ω -phase and α -phase parameters constant to refine the β phase, then holding the ω -phase and β -phase parameters constant to refine the α phase, and finally holding the β -phase and α -phase parameters constant to refine the ω phase. This process was repeated as necessary to complete the refinement. Phase volume fractions were also calculated as part of this Rietveld analysis, and can be found in Ballor et al. [42].

The a_{β} values of each alloy were found to decrease with increasing aging time, see Figure 6. The a_{β} values of the Fe-containing and the Fe-free alloys decrease at different rates; i.e. the decrease in a_{β} of TC and TCA were comparable and the decrease in a_{β} of TCF and TCFA were comparable. The Fe addition resulted in an increased a_{β} for all aging times. Due to the difficulty in refining certain profiles, some data scatter exists in the calculated lattice parameters of each phase.

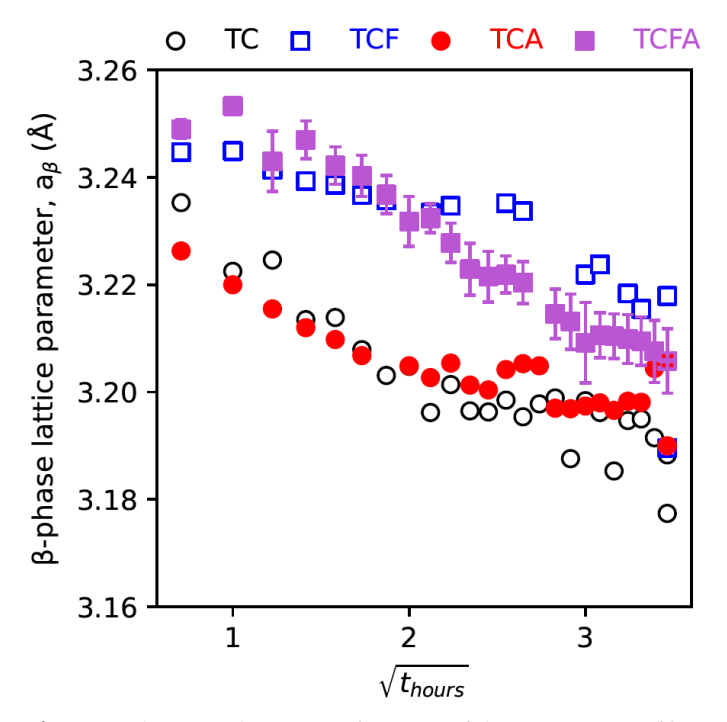


Figure 6. The $a\beta$ evolution as a function of the square root of hours aging.

The 'a' (a_{α}) and 'c' (c_{α}) lattice parameters and the corresponding c/a ratios of the α phase were plotted as a function of aging time for each alloy, see Figure 7. The a_{α} of TC and TCA are similar, and decrease following similar trends throughout the aging, and the a_{α} of TCF and TCFA are similar for shorter aging times (it is noted that significant scatter exists in the TCF data for longer aging times). The c_{α} of each alloy were similar (taking into account the data scatter). The c/a ratios of TCF and TCFA approached approximately 1.582 and 1.580, respectively after 12 h of aging, see Figure 7. TC approached approximately 1.588. Scatter in the TCA c_{α} values translated into scatter in the TCA c/a ratios, making it less clear which c/a ratio value TCA approached, but the general trend of the TCA c_{α} ratios appeared to be similar to that for TC. It is noted that the c/a ratio of the α phase in pure Ti is 1.587, and is marked with a dashed line on Figure 7 [43,44].

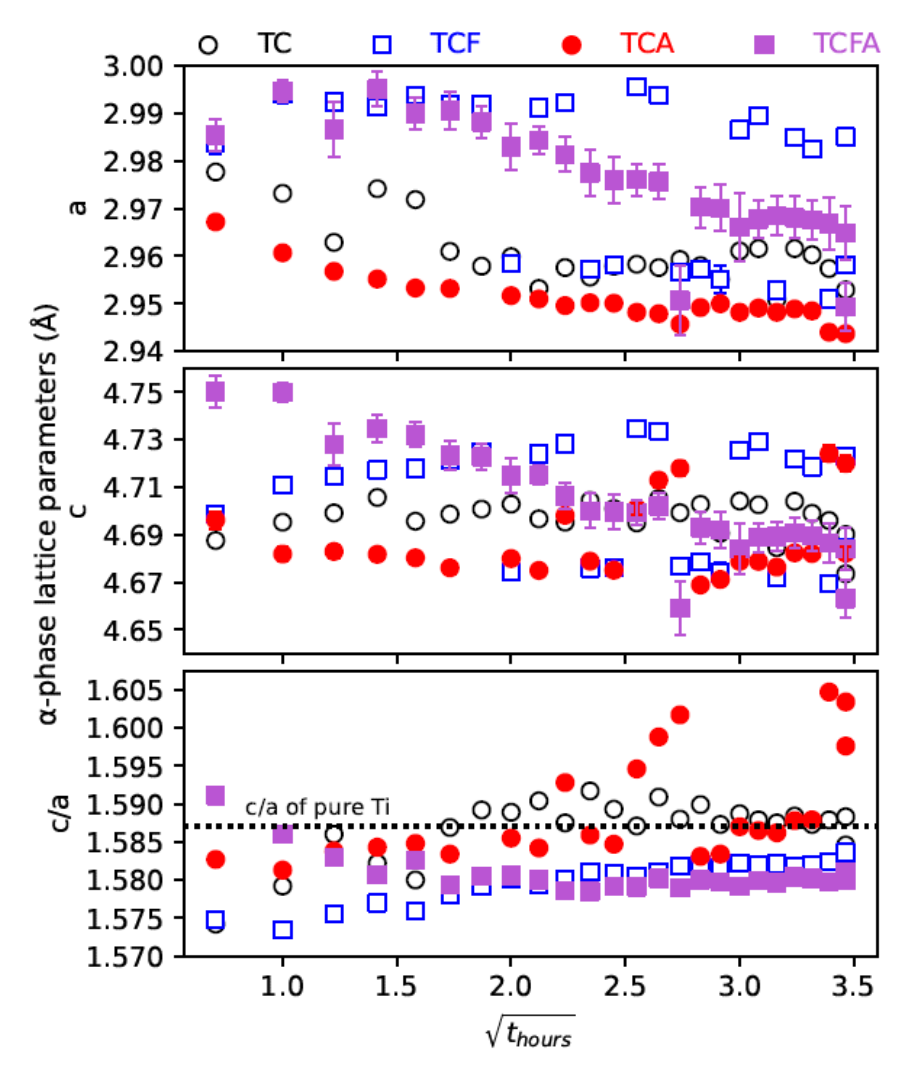


Figure 7. The α -phase lattice parameter evolution as a function of the square root of hours aging.

The 'a' (a ω) and 'c' (c ω) lattice parameters and the c/a ratios of the ω phase are plotted as a function of aging time for TC and TCF, respectively, see Figure 8. The a ω of TC decreases and the c ω of TC increases with increasing aging time, resulting in the c/a ratio of TC increasing from approximately 0.613 to approximately 0.622. The a ω , c ω , and c/a ratios of TCF remain relatively constant throughout the aging period, with the c/a ratio of TCF increasing slightly from approximately 0.612 to 0.613 during the 7.5 h that the ω phase was present. The lattice parameter values for TC and TF are within the range of lattice parameters reported for β -Ti and Zr alloys [45–49].

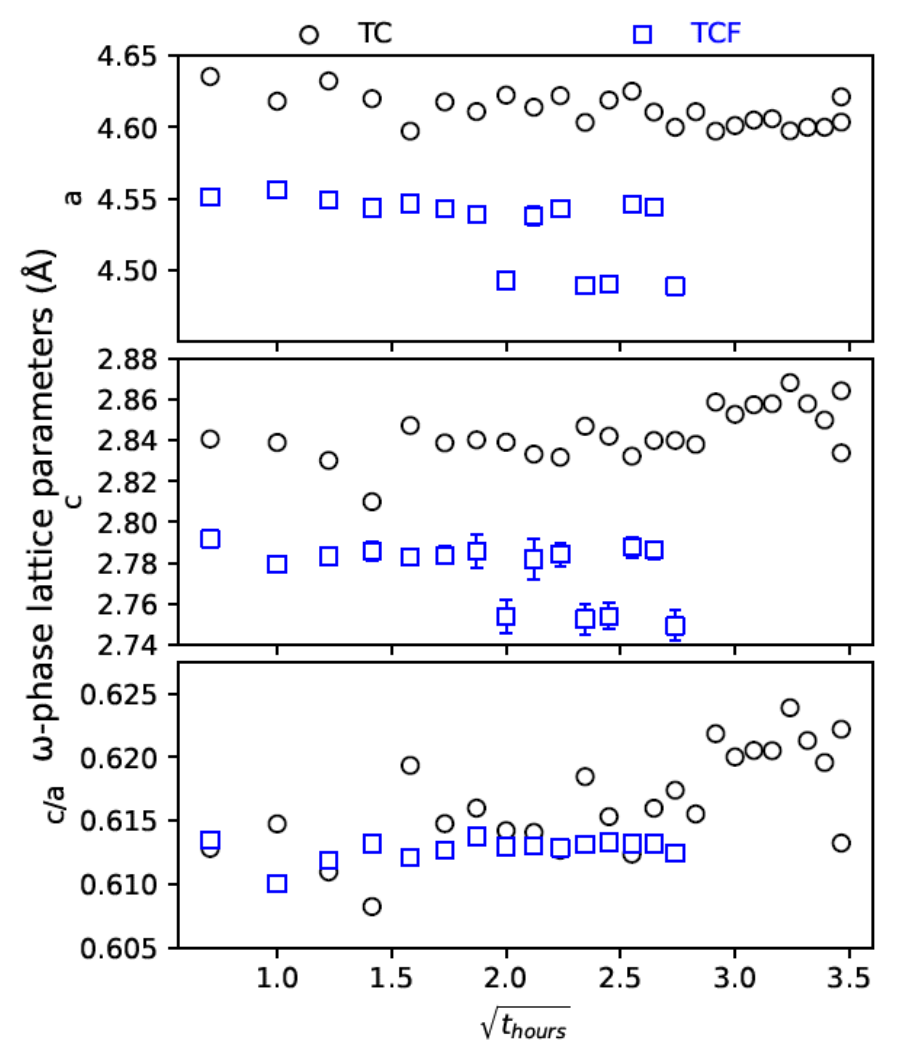


Figure 8. The ω -phase lattice parameter evolution as a function of the square root of hours aging.

3.2. Phase composition evolution evaluated by atom probe tomography

The precipitates in each alloy were poor in the β -phase stabilizing element Cr, so Cr isosurfaces were used to characterize the precipitates. Reconstructions of the TC, TCF, TCA, and TCFA samples after 0.75 h aging are shown along with their corresponding proximity histograms in Figure 9(a,b,c,d), respectively. The precipitates in the APT samples of TCA and TCFA were considered to be the α phase since the XRD results indicated that only the β and α phases are present in those alloys. SEM and TEM images of TCA and TCFA in Ballor et al. confirmed the lenticular morphology of the α phase precipitates in the β matrix [42]. The precipitates in the APT samples of TC and TCF are identified as either α or ω based on their morphology, where the lenticular or plate-shaped precipitates are considered to be the α phase, and the more equiaxed precipitates, resembling those found in Devaraj et al. [50], are considered to be the ω phase.

(a) TC (b) TCF (c) TCA (d) TCFA

Figure 9. APT tip reconstruction and the corresponding proximity histogram for (a) TC, (b) TCF, (c) TCA and (d) TCFA. All samples were aged at 400° C for 0.75 h. The vertical line shows the 8% Cr isoconcentration surface, and the dashed lines show the APT-measured compositions of the β-homogenized material reported in Ballor et al. [35].

The precipitates in TC and TCF consist almost entirely of Ti after 0.75 h of aging, as the β -stabilizers Cr and Fe diffused from the precipitates into the surrounding β matrix. The α -phase precipitates in TCA and TCFA are also β -stabilizer free after 0.75 h aging, but contain higher concentrations of the α -stabilizer Al than the surrounding β matrix, and lower Ti concentrations (by approximately 10%) in the α phase compared to the precipitates in TC and TCF. The datasets in Figure 9 are representative of the datasets collected for the alloys after each aging time, and the phase compositions for each aging time were calculated from the proximity histograms to determine the evolution of phase composition with aging time.

The β phase decreases in Ti content and increases in Cr content in each alloy, see Figure 10(a). In contrast, the compositions of the α and ω phases remain relatively

272

273

274

275

276

277

278

279

280

281

constant with increasing aging time, see Figure 10(b). The changes in the β -phase composition occurred because the β -phase stabilizers, Cr and Fe, diffuse from the α and ω phases into the β phase during their precipitation and growth, while the α -phase stabilizer, Al, diffuses into the α phase. In TCF, less Cr diffuses into the β phase than in TC, achieving 15.5 at.% compared to the 27 at.% achieved in TC after 12 h aging. It is noted that higher concentrations of the impurity element O were measured in the α phase than in the β phase in all samples. O was present in the α phase in average concentrations of 1.2±0.6%, while O was present in the β phase in average concentrations of 0.2±0.1% (the averages and standard deviations were taken from 18 samples). Because O is an impurity element, it was not included in the phase composition analysis as the starting O content of each sample, before the phase transformations occurred, was unknown.

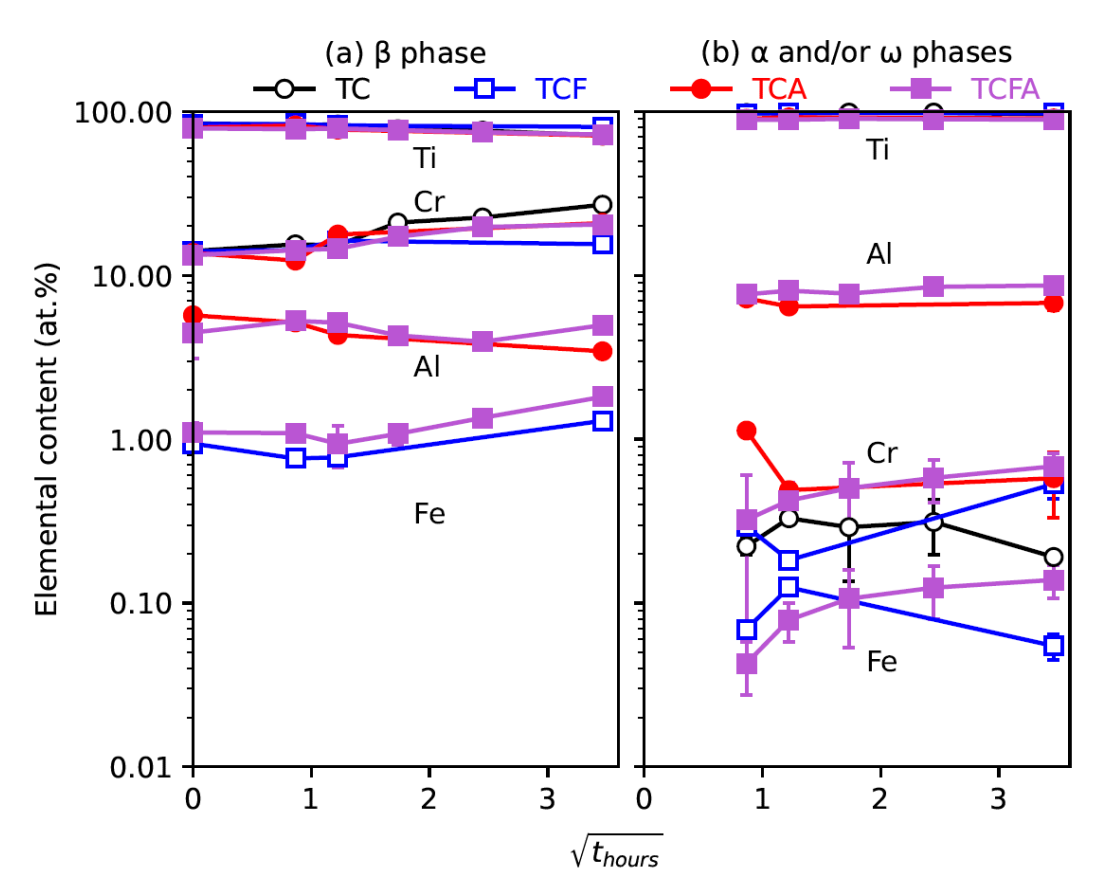


Figure 10. The APT measured Ti, Cr, Fe, and Al concentrations of the (a) β phase and (b) α and ω phases as a function of the square root of hours aging. Error bars indicate ±1 standard deviation, and for the cases when error bars were lacking, only one measurement was taken.

The ratios of the concentration of solute atoms Cr, Fe, and Al in the ω and/or α phases to the concentration of these solute atoms in the β phase were calculated, see Figure 11. Most of ratios for Cr fell between 0.01 and 0.03. TC and TCF exhibited slightly more variation in the ratios for Cr than TCA and TCFA. The ratios for Fe in TCF and TCFA were approximately 0.1. The ratios for Al in the α phase to the β phase in TCA and TCFA was approximately 1.5 throughout the aging treatment. These ratios can be compared to the partition coefficients during solidification described by Porter and Easterling, as they represent the ratios of solute atoms in the transforming phase compared to the parent phase [51]. However, some key differences should be noted. The partition coefficient described by Porter and Easterling compares solute compositions between the solidifying phase and the liquid phase, not between solid-solid phase transformations. Also, the partition coefficient is calculated from the equilibrium phase diagram, and the ω phase does not appear

311

on the equilibrium phase diagram of Ti-Cr alloys, making it difficult to directly compare the ratios for the ω -containing TC and TCF.

TCF

(b) Fe

TCA

(a) Cr

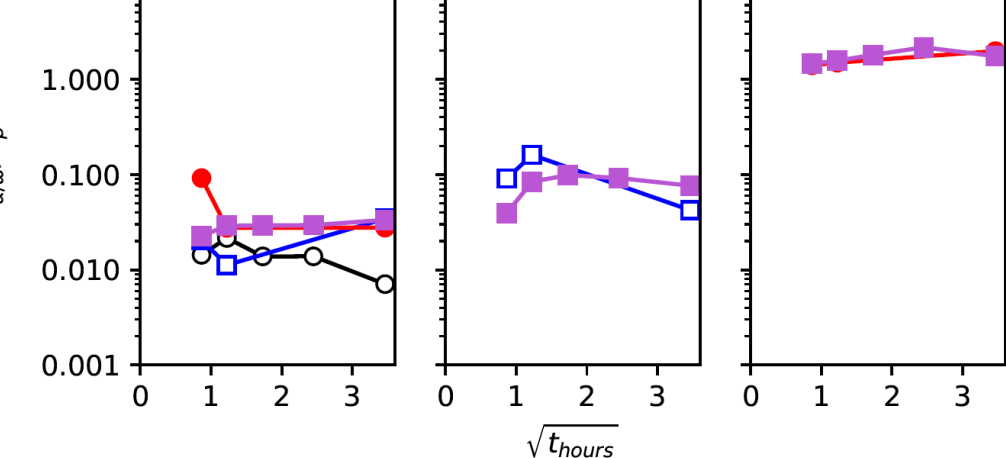


Figure 11. The ratios of the concentration of solute elements (a) Cr, (b) Fe, and (c) Al in the α and/or ω phases to the concentration of these solute elements in the β phase. The ratios are shown as a function of the square root of hours aging.

4. Discussion 316

4.1. The β phase

10.000

The a_{β} was expected to decrease linearly as the Cr and Fe concentrations in the β phase increased because Cr and Fe have smaller atomic radii as Ti, see Table 2. Linear relationships were exhibited between a_β and Mo-Eq, a_β and average atomic radius, and a_β and average Md, see Figure 12. The changes in a_{β} during the phase transformations were consistent with data from fully β-phase Ti alloys. The average atomic radius and average Md decreased as Mo-Eq increased, which was expected as the Md and atomic radii values of each alloying element are smaller than those of Ti, see Table 2.

Table 2. The atomic radii and electron d-shell energy (Md) for Ti, Cr, Fe, and Al in bcc Ti. The atomic radii are from Callister [52] and the Md values are from Morinaga et al. [53].

| Element | Atomic radius (Å) | Md (eV) | |
|---------|-------------------|---------|--|
| Ti | 1.45 | 2.447 | |
| Cr | 1.25 | 1.478 | |
| Fe | 1.24 | 0.969 | |
| Al | 1.43 | 2.200 | |

312 313

314

315

318 319

320

317

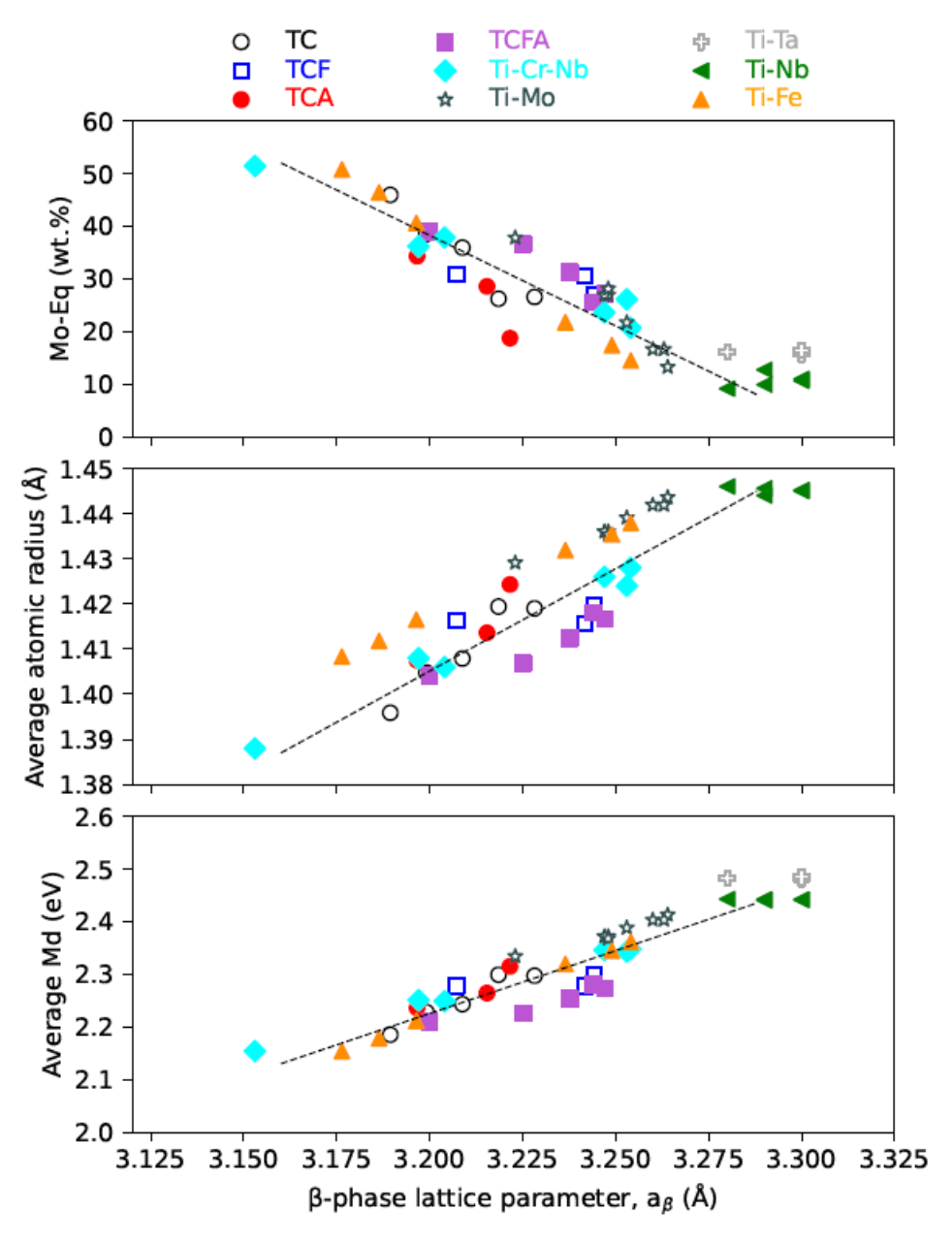


Figure 12. The β-phase lattice parameters (α β values) as a function of Mo-Eq (top), average atomic radius (middle), and average Md (bottom). Data were taken from this work and work involving Ti-Cr-Nb alloys [4], Ti-Fe alloys [5], Ti-Mo alloys [6], Ti-Ta alloys [7], and Ti-Nb alloys [7].

While distinct relationships between Mo-Eq, average Md, and average atomic radius exist for the Ti-Mo, Ti-Fe, Ti-Nb, and Ti-Cr-Nb alloys shown in Figure 1, more universal relationships appear to exist between each of those parameters and a_{β} . The agreement between the literature and the current work suggest that all β -Ti alloys should follow the relationships represented in Figure 12 during the aging phase transformations. These relationships are important as they could affect β -phase deformation mechanisms. Md, in particular, is useful for determining whether alloys will deform via slip or twinning [53], and a changing Md could indicate a changing deformation mechanism.

The composition changes during the 400°C aging could also affect the subsequent phase transformations. For example, a higher β -stabilizer concentration in the β matrix could favor the nucleation of new precipitates at phase boundaries over the growth of existing precipitates, which could assist in promoting the formation of nanoscale α phase at the ω/β boundary during the ω -assisted α -phase transformation. The decreasing a β

could also introduce strain at the α/β and/or ω/β boundaries, which could affect phase nucleation, growth, and morphology. The effect of a_β on the α and ω phases is discussed in detail below.

4.2. The α phase

As the α phase nucleates and grows in each alloy, its composition remained relatively constant (see Figure 10(b)), but the α -phase lattice parameters showed some change (see Figure 7). Thus, the relationships between lattice parameters (a_{α} and c_{α} and c_{α} ratio) were explored. TCFA showed the only statistically significant trends (R² above 0.99), with a_{α} , c_{α} , and the c_{α} ratio increasing as Cr and Fe decreased, and a_{α} , c_{α} , and the c_{α} ratio decreasing as Al concentration increased. The c_{α} ratios are presented in Figure 13 and the scatter is representative of both a_{α} and c_{α} . TC, TCF, and TCA did not exhibit any statistically significant relationships (all R² values were below 0.95). This suggests that composition does not directly influence α -phase lattice parameters through atomic radius differences, but could be facilitating α -phase lattice parameter change by changing a_{β} and inducing strain at the α/β boundary. To further explore the effects of composition, the relationships between a_{β} and the α -phase lattice parameters were explored.

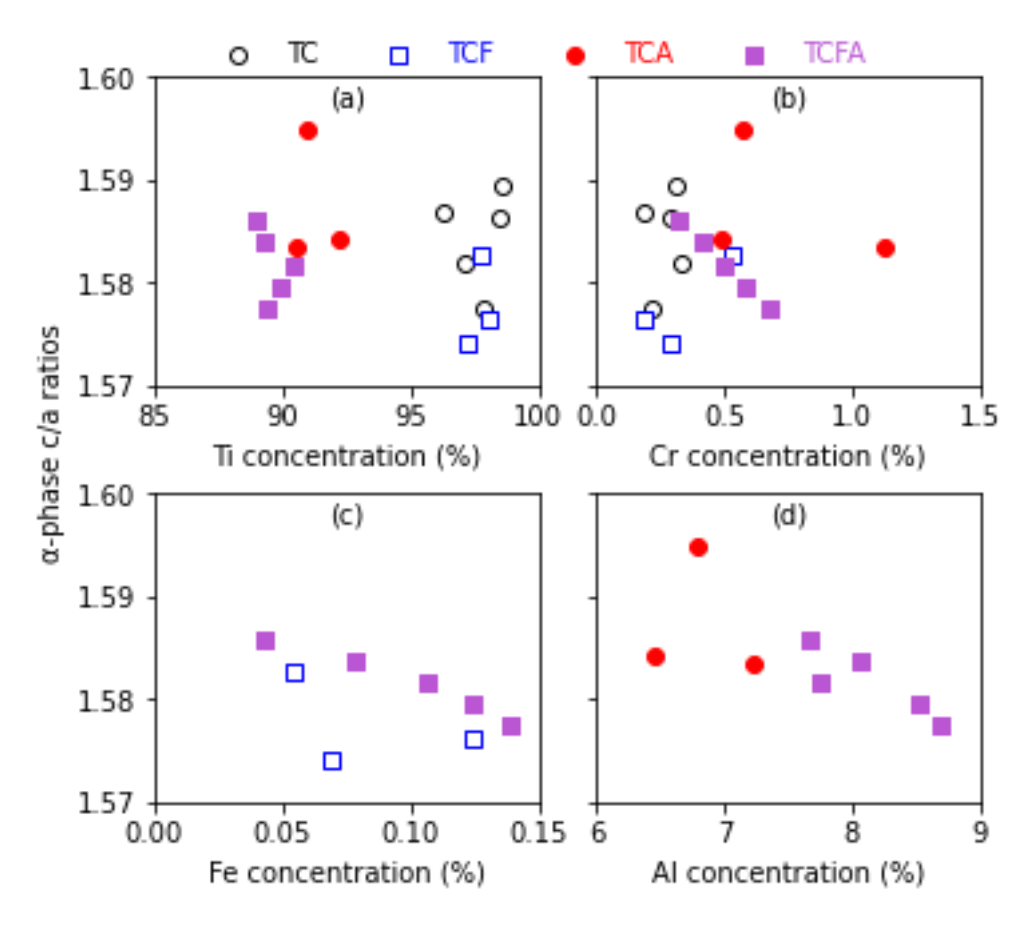


Figure 13. The α -phase c/a ratios of all alloys as a function of composition of (a) Ti, (b) Cr, (c) Fe, or (d) Al.

Both a_{α} and c_{α} decreased as a_{β} decreased, see Figure 14. The c/a ratios of TC and TCA both approached the c/a ratio of the α -phase in pure Ti (1.587 [43]). The c/a ratios of TCF and TCFA did not approach 1.587, instead approaching values of ~1.582 and ~1.580 respectively. This supports the idea that composition influences the α -phase lattice parameters through the changing a_{β} , as TC and TCA had similar a_{β} evolutions and TCF and TCFA had similar a_{β} evolutions.

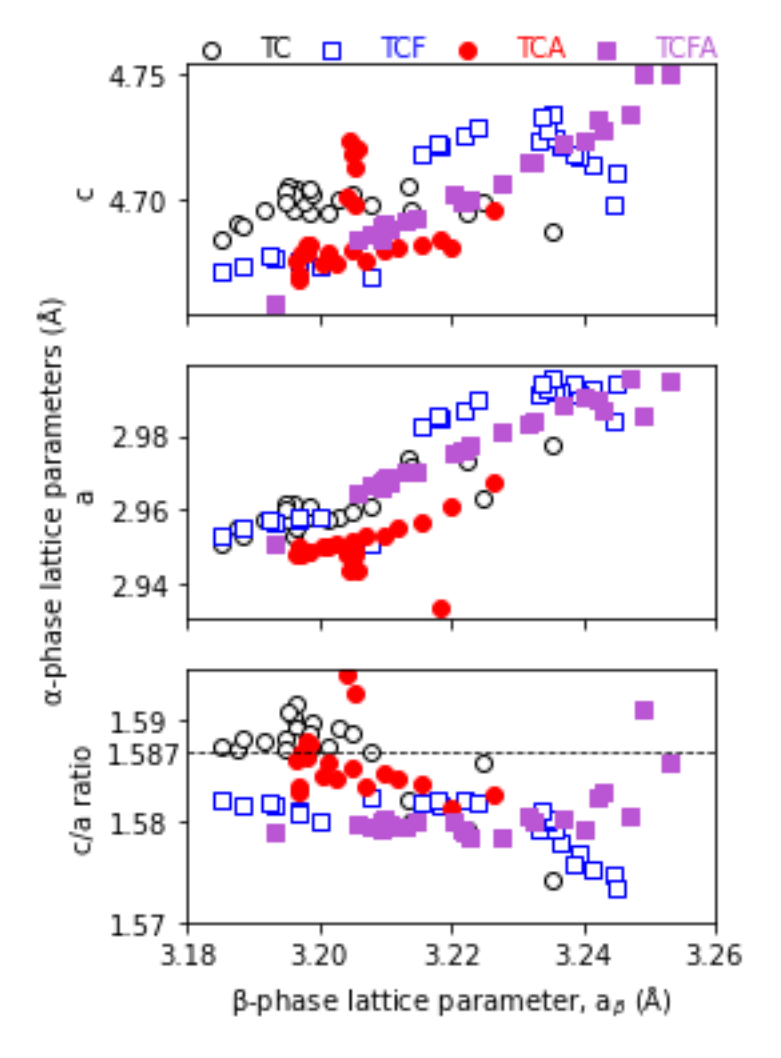


Figure 14. The α -phase lattice parameters c (top), a (middle), and c/a ratios (bottom) of TC, TCF, TCA, and TCFA as a function of a_β.

This relationship is significant as the misfit between the α and β phases and the coherency strains along the $(\bar{1}100)_{\alpha}$ and $(\bar{1}1\bar{2})_{\beta}$ planes, where the misfit between the α and β phases is minimized, could have been affected [54]. If the changing a_{β} and c/a ratio affect the misfit between the two phases, the ledges that transition the crystal from the α to the β phase could be affected. In particular, the ledges could become a more favorable location for the nucleation or growth of the α phase than the β -stabilizer-rich β -matrix, which could explain the clusters of α phase observed in the TCFA APT sample shown in Figure 9(d) and in the SEM micrographs in Ballor et al. [42]. Further investigation into the misfit and coherency strain between the α and β phases as a_{β} and the α -phase c/a ratio change during the β -to- α transformation would be valuable.

4.3. The ω phase

The ω -phase lattice parameters of TC and TCF were compared to Ti and Cr concentrations, and no clear relationships were found between concentration and a_{ω} , c_{ω} , or the c/a ratios. The c/a ratios are presented in Figure 15 and the scatter is representative of a_{ω} and c_{ω} , as well.

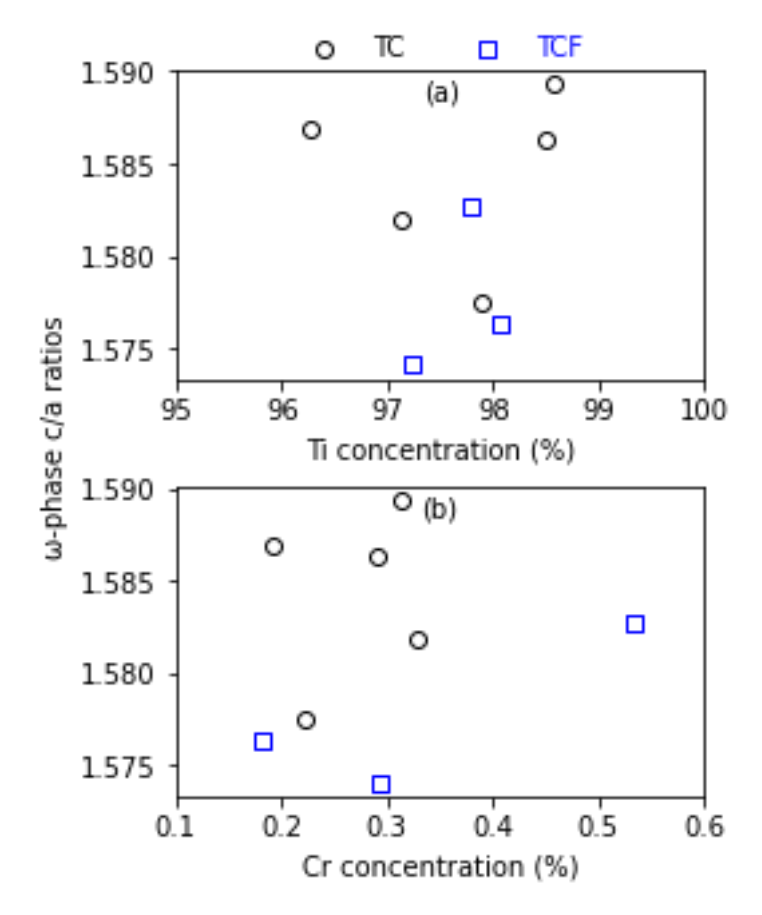


Figure 15. The ω -phase c/a ratios of TC and TCF as a function of composition of (a) Ti and (b) Cr.

Instead, like the α phase, the ω -phase parameters changed as the β -phase β -stabilizer content increased and a_{β} decreased. In TC, c_{ω} increased and a_{ω} decreased as a_{β} decreased. In TCF, both a_{ω} and c_{ω} decreased as a_{β} decreased. These changes result in an increased ω -phase c/a ratio for TC and an approximately constant c/a ratio for TCF, see Figure 15. This agrees with TC exhibiting a greater change in the β -phase Cr concentration than TCF, resulting in a greater change in a_{β} than TCF as well.

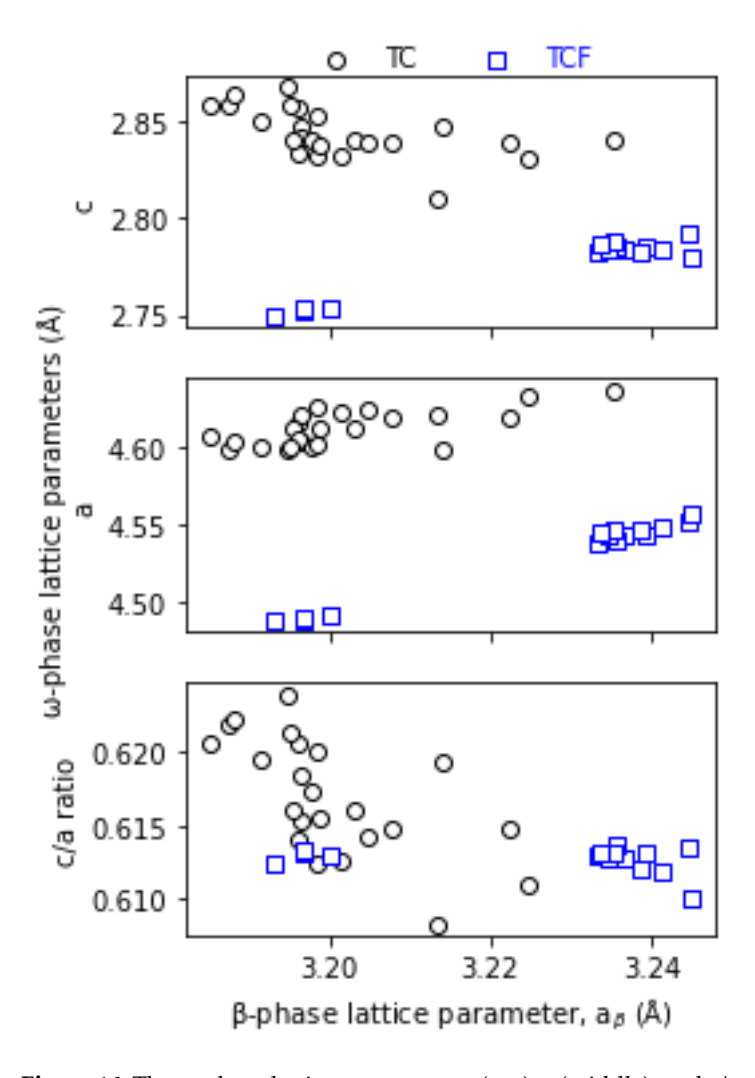


Figure 16. The ω -phase lattice parameters c (top), a (middle), and c/a ratios (bottom) for TC and TCF as a function of a_{β} .

This relationship is significant because the ω phase is known to change morphology from ellipsoidal to cuboidal as it grows and remains in the microstructure. The morphology of the ω phase is affected by the difference between the radii of the alloying elements and Ti [25,50], so the diffusion of the β -stabilizers with aging time would drive the ω -phase morphology to be more cuboidal. These results suggest that the morphology of the ω phase in TC changed from more ellipsoidal to more cuboidal during the aging process, while a change in ω phase morphology in TCF may not have occurred. More broadly, these results suggest that, along with aging time, the speed at which β -stabilizers diffuse in a β -Ti alloy could affect the ω -phase morphology during aging. This should be the focus of future study, as ω -phase morphology, ω/β boundary interfacial energy, and coherency strains at the ω/β interface all affect the ω -assisted α -phase transformation [26,27,55].

5. Conclusions

Fe- and Al-modified β -Ti alloys, each containing nominally 11at.% Cr, underwent a 400°C aging treatment to induce the β -to- ω and β -to- α phase transformations. The ω and α phases precipitated in TC and TCF during aging, while the 5.3at.% Al addition in TCA and TCFA inhibited ω -phase formation. During the phase transformations, the β -phase stabilizers Cr and Fe diffused from the α and ω phases into the β matrix, leaving the α and ω phases nearly β -phase stabilizer free. Ti diffused from the β -matrix into the α and ω phases, and the α -phase stabilizer Al diffused into the α phase. The β phase retained

some Al while being enriched with Cr and Fe. The β -phase lattice parameter decreased with increased Cr and Fe content during the phase transformations. The relationship between lattice parameter, atomic radius, Md, and Mo-Eq was explored. As Mo-Eq increased, the β -phase lattice parameter decreased with decreasing atomic radius and Md.

The α -phase lattice parameters exhibited a relationship with the β -phase lattice parameter and thus the β -phase composition. The c/a ratios of TC and TCA approached 1.587, and the c/a ratios of TCF and TCFA approached ~1.582 and ~1.580, respectively, as β -phase lattice parameter decreased. Similarly, the ω -phase lattice parameters exhibted a relationship with the β -phase lattice parameter and composition. TC exhibited larger composition changes, larger β -phase lattice parameter changes, and larger ω -phase lattice parameter changes than TCF. The ω -phase c/a ratio change suggests a change in ω -phase morphology during aging in TC. The smaller β -phase composition changes in TCF and an essentially constant ω -phase c/a ratio suggests no ω -phase morphology change.

The relationships between composition, β -phase lattice parameter, and the c/a ratios of the α and ω phases has implications for interfacial strain at the β/α or β/ω boundaries and the ω -assisted α -phase transformation. This work has shown that combining APT with HTXRD is a powerful means to systematically and accurately study compositional effects on lattice parameters. Overall, this work has provided important details of the interdependence of composition and the β -, α -, and ω -phase lattice parameters.

Supplementary Materials: There are no supplementary materials for this work.

Author Contributions: Conceptualization, J.B. and C.J.B.; methodology, J.B.; validation, X.X., Y.Y. and Z.Z.; formal analysis, J.B., J.D.P., and S.M.; investigation, J.B., J.D.P., and S.M.; resources, C.J.B., J.P., A.D., and S.M.; data curation, J.B., J.D.P., and S.M.; writing—original draft preparation, J.B.; writing—review and editing, J.B., C.J.B., A.D., J.D.P., and S.M.; visualization, J.B.; supervision, A.D. and C.J.B.; project administration, J.B. and C.J.B.; funding acquisition, C.J.B., S.M., and A.D. All authors have read and agreed to the published version of the manuscript.

Funding: This material is based in part on work supported by the U.S. Department of Energy, Office of Science, Office of Workforce Development for Teachers and Scientists, Office of Science Graduate Student Research (SCGSR) program. The SCGSR program is administered by the Oak Ridge Institute for Science and Education for the DOE under contract number DE-SC0014664. The funding for the alloy processing, metallographic preparation, and HTXRD was supported by National Science Foundation Division of Material Research (grant No. DMR1607942) through the Metals and Metallic Nanostructures (MMN) program. A portion of the funding for this research was supported by the U.S. Department of Energy, Office of Basic Energy Science through grant No. DE-SC0001525. A.D. would like to acknowledge the funding support from the Department of Energy, Office of Science, Basic Energy Sciences, Materials Sciences and Engineering Division as a part of the Early Career Research Program FWP 76052. S.M. acknowledges support via the Inamori Professorship which supported the in-situ XRD measurements and analysis. Please add: "This research received no external funding" or "This research was funded by NAME OF FUNDER, grant number XXX" and "The APC was funded by XXX". Check carefully that the details given are accurate and use the standard spelling of funding agency names at https://search.crossref.org/funding. Any errors may affect your future funding.

Data Availability Statement: The data presented in this study are available on request from the corresponding author. The data are subject to an approval for release process.

Acknowledgments: The authors would like to thank Swavek Zdzieszynski for assistance in performing the HTXRD experiments and James Burns for assistance in performing APT sample preparation and running the APT experiments. The APT research was supported by the Center for Nanophase Materials Sciences (CNMS), which is a US Department of Energy, Office of Science User Facility at Oak Ridge National Laboratory and the Environmental Molecular Sciences Laboratory, a national scientific user facility sponsored by the Department of Energy's Office of Biological and environmental Research located at Pacific Northwest National Laboratory. The authors acknowledge Dr. Masahiko Ikeda of Kansai University for donating the materials studied and useful insights, Dr. Elizabeth Kautz of North Carolina State University for helpful discussions about the APT data, and Dr. Alexandra Zevalkink of Michigan State University for helpful discussions about the Rietveld analysis.

Conflicts of Interest: The authors declare no conflict of interest.

472

References 474

1. Cotton, J.D.; Briggs, R.D.; Boyer, R.R.; Tamirisakandala, S.; Russo, P.; Shchetnikov, N.; Fanning, J.C. State of the Art in Beta Titanium Alloys for Airframe Applications. *JOM* **2015**, *67*, 1281–1303, doi:10.1007/s11837-015-1442-4.

- 2. Faller, K.; (Sam) Froes, F.H. The Use of Titanium in Family Automobiles: Current Trends. *JOM* **2001**, *53*, 27–28, doi:10.1007/s11837-001-0143-3.
- 3. Bania, P.J. Beta Titanium Alloys and Their Role in the Titanium Industry. *JOM* **1994**, 46, 16–19, doi:10.1007/BF03220742.
- 4. Slokar, L.; Matković, T.; Matković, P. Alloy Design and Property Evaluation of New Ti–Cr–Nb Alloys. *Materials & Design* **2012**, *33*, 26–30, doi:10.1016/j.matdes.2011.06.052.
- 5. Levinger, B.W. Lattice Parameter of Beta Titanium at Room Temperature. *JOM* **1953**, *5*, 195–195, doi:10.1007/BF03397474.
- 6. Hake, R.R.; Leslie, D.H.; Berlincourt, T.G. Electrical Resistivity, Hall Effect and Superconductivity of Some b.c.c. Titanium-Molybdenum Alloys. *Journal of Physics and Chemistry of Solids* **1961**, 20, 177–186, doi:10.1016/0022-3697(61)90002-6.
- 7. Kim, H.Y.; Miyazaki, S. Chapter 1 Martensitic Transformation Characteristics. In *Ni-Free Ti-Based Shape Memory Alloys*; Kim, H.Y., Miyazaki, S., Eds.; Butterworth-Heinemann, 2018; pp. 1–52 ISBN 978-0-12-809401-3.
- 8. Kim, H.Y.; Ikehara, Y.; Kim, J.I.; Hosoda, H.; Miyazaki, S. Martensitic Transformation, Shape Memory Effect and Superelasticity of Ti–Nb Binary Alloys. *Acta Materialia* **2006**, *54*, 2419–2429, doi:10.1016/j.actamat.2006.01.019.
- 9. Coakley, J.; Radecka, A.; Dye, D.; Bagot, P.A.J.; Stone, H.J.; Seidman, D.N.; Isheim, D. Isothermal Omega Formation and Evolution in the Beta-Ti Alloy Ti-5Al-5Mo-5V-3Cr. *Philosophical Magazine Letters* **2016**, *96*, 416–424, doi:10.1080/09500839.2016.1242877.
- 10. Devaraj, A.; Joshi, V.V.; Srivastava, A.; Manandhar, S.; Moxson, V.; Duz, V.A.; Lavender, C. A Low-Cost Hierarchical Nanostructured Beta-Titanium Alloy with High Strength. *Nat Commun* **2016**, *7*, 11176, doi:10.1038/ncomms11176.
- 11. Paiotti Marcondes Guimarães, R.; Callegari, B.; Warchomicka, F.; Aristizabal, K.; Soldera, F.; Mücklich, F.; Cavalcanti Pinto, H. In Situ Analysis of the Phase Transformation Kinetics in the β-Water-Quenched Ti-5Al-5Mo-5V-3Cr-1Zr Alloy during Ageing after Fast Heating. *QuBS* **2020**, *4*, 12, doi:10.3390/qubs4010012.
- 12. Szkliniarz, W.; Smołka, G. Analysis of Volume Effects of Phase Transformation in Titanium Alloys. *Journal of Materials Processing Technology* **1995**, *53*, 413–422, doi:https://doi.org/10.1016/0924-0136(95)01998-T.
- 13. Barriobero-Vila, P.; Requena, G.; Buslaps, T.; Alfeld, M.; Boesenberg, U. Role of Element Partitioning on the α - β Phase Transformation Kinetics of a Bi-Modal Ti-6Al-6V-2Sn Alloy during Continuous Heating. *Journal of Alloys and Compounds* **2015**, *626*, 330–339, doi:10.1016/j.jallcom.2014.11.176.
- 14. de Fontaine, D.; Paton, N.E.; Williams, J.C. The Omega Phase Transformation in Titanium Alloys as an Example of Displacement Controlled Reactions. *Acta Metallurgica* **1971**, *19*, 1153–1162.
- 15. Li, M.; Min, X. Origin of ω-Phase Formation in Metastable β-Type Ti-Mo Alloys: Cluster Structure and Stacking Fault. *Sci Rep* **2020**, *10*, 8664, doi:10.1038/s41598-020-65254-z.
- 16. Enzinger, R.J.; Luckabauer, M.; Okamoto, N.L.; Ichitsubo, T.; Sprengel, W.; Würschum, R. Influence of Oxygen on the Kinetics of Omega and Alpha Phase Formation in Beta Ti–V. *Metall Mater Trans A* **2023**, *54*, 473–486, doi:10.1007/s11661-022-06881-1.
- 17. Brumbauer, F.; Okamoto, N.L.; Ichitsubo, T.; Sprengel, W.; Luckabauer, M. Minor Additions of Sn Suppress the Omega Phase Formation in Beta Titanium Alloys. *Acta Materialia* **2024**, 262, 119466, doi:10.1016/j.actamat.2023.119466.

- 18. Mukherjee, R.; Abinandanan, T.A.; Gururajan, M.P. Phase Field Study of Precipitate Growth: Effect of Misfit Strain and Interface Curvature. *Acta Materialia* **2009**, *57*, 3947–3954, doi:10.1016/j.actamat.2009.04.056.
- 19. Grant, B.M.B.; Knoche, E.; Preuss, M.; da Fonseca, J.Q.; Daymond, M.R. The Effect of Lattice Misfit on Deformation Mechanisms at High Temperature. *AMR* **2011**, *278*, 144–149, doi:10.4028/www.scientific.net/AMR.278.144.
- 20. Chen, P.; Wang, F.; Li, B. Misfit Strain Induced Phase Transformation at a Basal/Prismatic Twin Boundary in Deformation of Magnesium. *Computational Materials Science* **2019**, 164, 186–194, doi:10.1016/j.commatsci.2019.04.020.
- 21. Yilbas, B.S. Laser Duplex Treatment of Surfaces for Improved Properties. In *Comprehensive Materials Processing*; Elsevier, 2014; p. 286 ISBN 978-0-08-096533-8.
- 22. Prevey, P.S. X-Ray Diffraction Residual Stress Techniques. In *Metals Handbook*; Metals Park: American Society for Metals, 1986; pp. 380–392.
- 23. Zheng, Y.; Williams, R.E.A.; Wang, D.; Shi, R.; Nag, S.; Kami, P.; Sosa, J.M.; Banerjee, R.; Wang, Y.; Fraser, H.L. Role of ω Phase in the Formation of Extremely Refined Intragranular α Precipitates in Metastable β-Titanium Alloys. *Acta Materialia* **2016**, 103, 850–858, doi:10.1016/j.actamat.2015.11.020.
- 24. Zheng, Y.; Williams, R.E.A.; Sosa, J.M.; Wang, Y.; Banerjee, R.; Fraser, H.L. The Role of the ω Phase on the Non-Classical Precipitation of the α Phase in Metastable β-Titanium Alloys. *Scripta Materialia* **2016**, *111*, 81–84, doi:10.1016/j.scriptamat.2015.08.019.
- 25. Duerig, T.W.; Terlinde, G.T.; Williams, J.C. Phase Transformations and Tensile Properties of Ti-10V-2Fe-3AI. *MTA* **1980**, *11*, 1987–1998, doi:10.1007/BF02655118.
- 26. Shi, R.; Zheng, Y.; Banerjee, R.; Fraser, H.L.; Wang, Y. ω -Assisted α Nucleation in a Metastable β Titanium Alloy. *Scripta Materialia* **2019**, *171*, 62–66, doi:10.1016/j.scriptamat.2019.06.020.
- 27. Li, T.; Kent, D.; Sha, G.; Liu, H.; Fries, S.G.; Ceguerra, A.V.; Dargusch, M.S.; Cairney, J.M. Nucleation Driving Force for ω-Assisted Formation of α and Associated ω Morphology in β-Ti Alloys. *Scripta Materialia* **2018**, *155*, 149–154, doi:10.1016/j.scriptamat.2018.06.039.
- 28. Sadeghpour, S.; Abbasi, S.M.; Morakabati, M.; Bruschi, S. Correlation between Alpha Phase Morphology and Tensile Properties of a New Beta Titanium Alloy. *Materials & Design* **2017**, 121, 24–35, doi:10.1016/j.matdes.2017.02.043.
- 29. Azimzadeh, S.; Rack, H.J. Phase Transformations in Ti-6.8Mo-4.5Fe-1.5Al. *Metall and Mat Trans A* **1998**, 29, 2455–2467, doi:10.1007/s11661-998-0217-8.
- 30. Hsu, H.-C.; Wu, S.-C.; Hsu, S.-K.; Li, C.-T.; Ho, W.-F. Effects of Chromium Addition on Structure and Mechanical Properties of Ti–5Mo Alloy. *Materials & Design* (1980-2015) **2015**, 65, 700–706, doi:10.1016/j.matdes.2014.09.077.
- 31. Ho, W.-F.; Pan, C.-H.; Wu, S.-C.; Hsu, H.-C. Mechanical Properties and Deformation Behavior of Ti–5Cr–xFe Alloys. *Journal of Alloys and Compounds* **2009**, 472, 546–550, doi:10.1016/j.jallcom.2008.05.015.
- 32. Silcock, J.M. An X-Ray Examination of the ω Phase in TiV, TiMo and TiCr Alloys. *Acta Metallurgica* **1958**, *6*, 481–493.
- 33. Chandrasekaran, V.; Taggart, R.; Polonis, D.H. An Electron Microscopy Study of the Aged Omega Phase in Ti-Cr
 Alloys. *Metallography* **1978**, *11*, 183–198, doi:10.1016/0026-0800(78)90035-6.
- 34. Murray, J.L. *Phase Diagrams of Binary Titanium Alloys*; Monograph series on alloy phase diagrams; ASM 553 International: Metals Park, Ohio, 1987; ISBN 0-87170-248-7.
- 35. Ballor, J.; Ikeda, M.; Kautz, E.J.; Boehlert, C.J.; Devaraj, A. Composition-Dependent Microstructure-Property

 Relationships of Fe and Al Modified Ti-12Cr (Wt.%). *JOM* **2019**, *71*, 2321–2330, doi:10.1007/s11837-019-03467-y.

 556

- 36. Gammon, L.M.; Briggs, R.D.; Packard, J.M.; Batson, K.W.; Boyer, R.; Domby, C.W. Metallography and Microstructures of Titanium and Its Alloys. In *Metallography and Microstructures*; Vander Voort, G.F., Ed.; ASM International, 2004; pp. 899–917 ISBN 978-1-62708-177-1.
- 37. Devaraj, A.; Perea, D.E.; Liu, J.; Gordon, L.M.; Prosa, Ty.J.; Parikh, P.; Diercks, D.R.; Meher, S.; Kolli, R.P.; Meng, Y.S.; et al. Three-Dimensional Nanoscale Characterisation of Materials by Atom Probe Tomography. *International Materials Reviews* **2018**, *63*, 68–101, doi:10.1080/09506608.2016.1270728.
- 38. Rigaku Integrated X-Ray Powder Diffraction Software PDXL. Rigaku Journal 2010, 26, 23–27.
- 39. Taylor, J.L.; Duwez, P. Trans. Amer. Soc. Met. 1952, 44.
- 40. Pawar, R.R.; Deshpande, V.T. Acta Crystallogr., Sec.
- 41. Chebotareva, Ye.S.; Nuzhdina, S.G. Phys. Met. Metall. 1973, 36.
- 42. Ballor, J.; Shawon, A.A.; Zevalkink, A.; Sunaoshi, T.; Misture, S.; Boehlert, C.J. The Effects of Fe and Al on the Phase Transformations and Mechanical Behavior of β-Ti Alloy Ti-11at.%Cr. *Materials Science and Engineering: A* **2023**, *886*, 145677, doi:10.1016/j.msea.2023.145677.
- 43. Lütjering, G.; Williams, J.C. *Titanium*; 2nd ed.; Springer: Berlin, 2007; ISBN 978-3-540-71397-5.
- 44. Jaffee, R.I. The Physical Metallurgy of Titanium Alloys. *Progress in Metal Physics* **1958**, 7, 65–163, doi:https://doi.org/10.1016/0502-8205(58)90004-2.
- 45. Hickman, B.S. The Formation of Omega Phase in Titanium and Zirconium Alloys: A Review. *J Mater Sci* **1969**, 4, 554–563, doi:10.1007/BF00550217.
- 46. Silcock, J.M.; Davies, M.H.; Hardy, H.K. Structure of the ω-Precipitate in Titanium–16 per Cent Vanadium Alloy. *Nature* **1955**, *175*, 731.
- 47. Aurelio, G.; Fernández Guillermet, A. Interatomic Distances of the Hexagonal Omega Structure in Ti-V Alloys: Neutron Diffraction Study and Analysis of Bonding Related Regularities. *Scripta Materialia* **2000**, 43, 665–669, doi:10.1016/S1359-6462(00)00457-7.
- 48. Bönisch, M.; Panigrahi, A.; Stoica, M.; Calin, M.; Ahrens, E.; Zehetbauer, M.; Skrotzki, W.; Eckert, J. Giant Thermal Expansion and α-Precipitation Pathways in Ti-Alloys. *Nat Commun* **2017**, *8*, 1429, doi:10.1038/s41467-017-01578-1.
- 49. Hatt, B.A.; Roberts, J.A. The W-Phase in Zirconium Base Alloys. *Acta Metallurgica* **1960**, *8*, 575–584.
- 50. Devaraj, A.; Williams, R.E.A.; Nag, S.; Srinivasan, R.; Fraser, H.L.; Banerjee, R. Three-Dimensional Morphology and Composition of Omega Precipitates in a Binary Titanium–Molybdenum Alloy. *Scripta Materialia* **2009**, *61*, 701–704, doi:10.1016/j.scriptamat.2009.06.006.
- 51. Porter, D.A.; Easterling, K.E. *Phase Transformations in Metals and Alloys*; 2nd ed.; CRC Press, Taylor and Francis Group, 1992; ISBN 0-7487-5741-4.
- 52. William D. Callister, Jr. *Materials Science and Engineering An Introduction*; 5th ed.; John Wiley & Sons, Inc.: New York, 2000; ISBN 0-471-32013-7.
- 53. Morinaga, M.; Murata, Y.; Yukawa, H. Molecular Orbital Approach to Alloy Design. In *Applied Computational*590

 Materials Modeling; 2007; pp. 255–306 ISBN 978-0-387-23117-4.
 591
- 54. Zheng, Y.; Williams, R.E.A.; Viswanathan, G.B.; Clark, W.A.T.; Fraser, H.L. Determination of the Structure of α -β 592 Interfaces in Metastable β-Ti Alloys. *Acta Materialia* **2018**, *150*, 25–39, doi:10.1016/j.actamat.2018.03.003.
- 55. Nag, S.; Banerjee, R.; Fraser, H.L. Intra-Granular Alpha Precipitation in Ti–Nb–Zr–Ta Biomedical Alloys. *J Mater Sci* 2009, 44, 808–815, doi:10.1007/s10853-008-3148-2.